PHYSICAL REVIEW B VOLUME 43, NUMBER 10 1 APRIL 1991

Heat capacity and entropy of nonstoichiometric magnetite $Fe_{3(1-\delta)}O_4$: The thermodynamic nature of the Verwey transition

J. P. Shepherd*
Department of Physics, Purdue University, West Lafayette, Indiana 47907

J. W. Koenitzer and R. Aragón†
Department of Chemistry, Purdue University, West Lafayette, Indiana 47907

J. Spałek‡
Department of Physics, Purdue University, West Lafayette, Indiana 47907

J. M. Honig
Department of Chemistry, Purdue University, West Lafayette, Indiana 47907
(Received 10 September 1990)

The heat capacity of $Fe_{3(1-\delta)}O_4$, was systematically measured for nine samples in the composition range $0<\delta<0.012$ and for temperatures between 5 and 200 K. The character of the heat-capacity anomaly at the Verwey transition changed at $\delta=\delta_c\approx 0.004$: for $\delta<\delta_c$ or $\delta>\delta_c$ the transformation was of first or second order, respectively. The transition disappears altogether for $\delta>3\delta_c\simeq 0.012$. From these measurements the entropy of the transition and the temperature dependence of the entropy have been calculated. The entropy change at the transition is R ln2 for $\delta=0$ and decreases steadily with increasing δ. The implications of these findings are discussed in terms of a mean-field model that includes the Coulomb interactions among electrons located on neighboring octahedral sites. The charge carriers resonate between the two equivalent octahedral positions above the Verwey transition, and freeze out well below the transition. The model predicts a molar entropy change of R ln2 for discontinuous transitions and $2R$ ln2 for continuous transitions.

I. INTRODUCTION

The Verwey transition in magnetite has been the subject of many prior investigations; it has only gradually been recognized that the experimental data depend critically on the oxygen-to-iron ratio. In $Fe_{3(1-\delta)}O_4$ the δ parameter falls in the range $-0.0006<\delta<0.0125$; various physical properties such as heat capacity, electrical conductivity, magnetization, spin resonance, and Mössbauer spectra change drastically with δ. Accordingly, it is important to provide a reliable data base that describes those variations as a foundation for an adequate theoretical interpretation of these observed features.

The main purpose of this paper is to provide a systematic thermodynamic characterization of the Verwey transition. For this purpose we describe a set of extensive heat-capacity (C_p) measurements from which the temperature variations of the entropy for magnetite with variable δ can be determined. These results will then be described in terms of a simple theoretical model of collective electron behavior. This work represents an extension of earlier studies in this laboratory[1,2] on the heat capacity of near-stoichiometric magnetite ($\delta\approx 0$). Preliminary C_p measurements on nonstoichiometric magnetite have been briefly reported both for the temperature range 5–200 K (Ref. 3) and in the cryogenic region 0.3–20 K (Ref. 4).

Background information regarding calorimetric measurements for 1926–1984 was provided in Ref. 1, hereafter designated as I. Most of those investigations centered on the heat-capacity anomalies associated with the Verwey transition near 120 K. In many cases, the results serve only as a qualitative thermodynamic indicator of the transition because insufficient care was exercised in ensuring proper stochiometry and homogeneity of the sample and in eliminating major impurities. The need for adequate precautions is clearly apparent in the present study: with increasing cation deficiency, the Verwey transition temperature decreases significantly and the thermodynamic character of the transition is also altered. As far as is known, this is the first systematic calorimetric investigation on $Fe_{3(1-\delta)}O_4$ that covers almost the entire accessible stability range of magnetite between the reduction boundary (wüstite-magnetite) and the oxidation boundary (hematite-magnetite). The present results also indicate a significant change in the entropy of the transition as a function of the nonstoichiometry parameter δ.

II. EXPERIMENTAL TECHNIQUE

The preparation of homogeneous single crystals of magnetite was described in detail in I and in Ref. 5 and will only be briefly summarized. To ensure uniformity of composition, single crystals grown by the skull-melter technique were subjected to subsolidus anneals in appropriate CO-CO_2 buffered atmospheres in the range 10^{-12}–10^{-3} atm. The oxygen fugacity (f_{O_2}) was moni-

tored directly using a zirconia-yttria oxygen-transfer cell. The appropriate f_{O_2} value required to attain a desired δ in $Fe_{3(1-\delta)}O_4$ at a specified temperature was determined from Dieckmann's thermogravimetric data.[6] Annealing times were based on Dieckmann and Schmalzried's work[7] pertaining to tracer diffusion coefficients, and on numerical calculations involving Fick's second law for a semi-infinite slab.[8] For samples with $\delta > 0.004$, it was necessary to carry out subsolidus annealing at 1400 °C, followed by rapid quenching in a vertical drop furnace; the exterior portions of these samples were then trimmed off to achieve uniformity of composition of the core. Samples for which $\delta < 0.004$ were annealed at 1000 °C for several days and slow cooled; surface layers were removed by abrasion.

Samples approximately $5 \times 5 \times 0.7$ mm^3 in size, weighing between 40 and 80 mg, were obtained from the annealed crystals; they were polished, and mounted in a relaxation calorimeter designed by Griffing and Shivashankar.[9] The equipment could be operated in the relaxation mode for heat-capacity measurements or in a transition mode to obtain the enthalpy of transition. Temperatures were measured with a Ga-As-P diode[10] calibrated against a Ge or Pt resistance thermometer in the range 4.2–100 K or 75–350 K, respectively. The instrument was successfully checked for accuracy by measurement of the heat capacity of Cu metal and by monitoring the latent heat of freezing of Hg.

III. RESULTS

The temperature dependence of heat capacity is summarized in Figs. 1 and 2 for $Fe_{3(1-\delta)}O_4$ samples with $\delta < 0.004$ and $\delta > 0.004$, respectively. These two sets encompass the two regimes in which thermodynamically discontinuous and continuous Verwey transitions take place. Figure 3 displays a typical cooling curve for a representative sample with $\delta = 0.0017$ in the vicinity of its

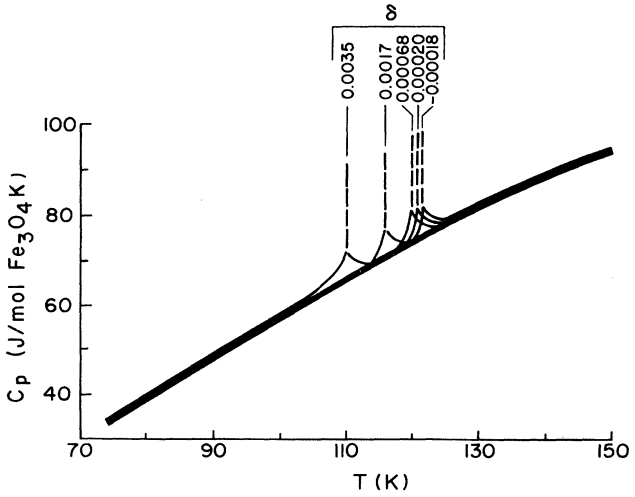

FIG. 1. Heat capacity vs temperature ($70 < T < 150$ K) for $Fe_{3(1-\delta)}O_4$ samples with $\delta < \delta_c \approx 0.004$, exhibiting first-order Verwey transitions.

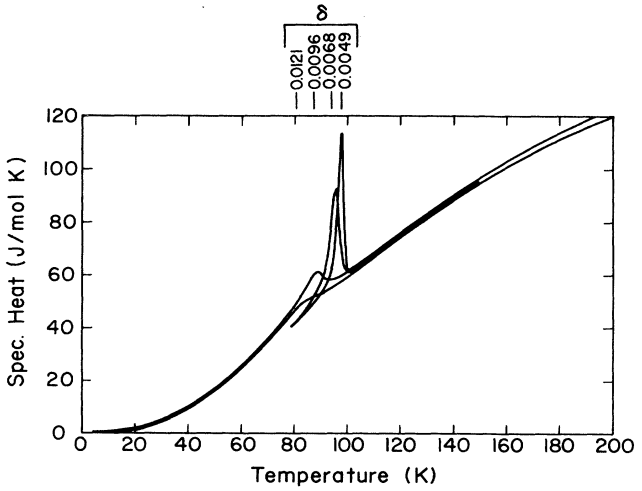

FIG. 2. Heat capacity vs temperature ($0 < T < 200$ K) for $Fe_{3(1-\delta)}O_4$ samples with $\delta_c < \delta < 0.012$, exhibiting higher-order Verwey transitions.

first-order phase transition near 114.8 K. The first-order nature of transition is reflected by the nearly flat thermal arrest (plateau); the latent enthalpy of the transition was calculated as described elsewhere.[2] This arrest corresponds to a very sharp C_p spike in Fig. 1 which is superposed on the background of a continuous variation in heat capacity with temperature.

Figure 4 shows the temperature dependence of the excess heat capacity ΔC_p for a sample with $\delta = 0.0096$ undergoing a continuous Verwey transition that is centered on $T_V \simeq 89$ K. The corresponding heating or cooling curves exhibit no thermal-arrest features. There is some uncertainty in the ΔC_p versus T plot of Fig. 4 because judgmental factors are involved in drawing the baseline. In particular, differences between the baseline and observed heat capacities should extend down to 0 K in all second-order transitions. However, the general shape of the ΔC_p curve remains unaffected by this difficulty. As is seen, the heat-capacity anomaly now extends over a wide temperature range centered on T_V. Additional heat-

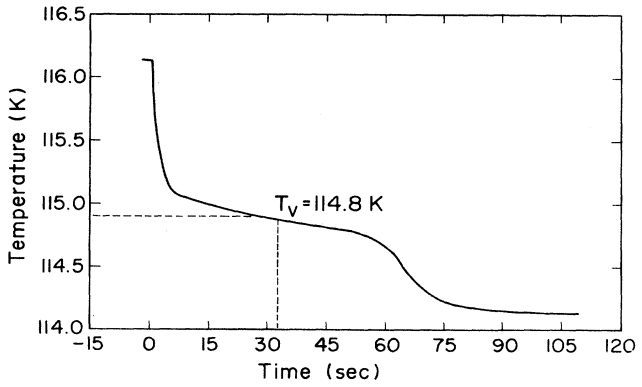

FIG. 3. Cooling curve for $Fe_{3(1-\delta)}O_4$ with $\delta = 0.0017$ in the vicinity of the Verwey transition. Note temperature scale.

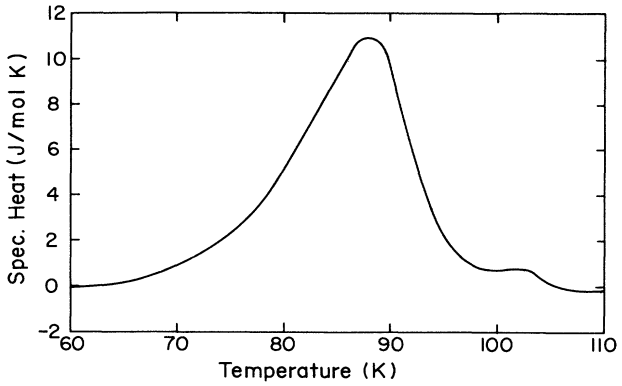

FIG. 4. Excess specific heat of $Fe_{3(1-\delta)}O_4$ with $\delta=0.0096$ near the Verwey transition.

capacity data and heating or cooling curves for other δ values of magnetite were already presented in Refs. 2 and 3 and will not be duplicated here.

One important conclusion to be drawn from the above data, in conformity with our earlier report,[3] is that a drastic change in the nature at the Verwey transition takes place for $\delta=\delta_c\simeq 0.004$. For the composition range $-0.0005<\delta<\delta_c$ (group-I specimens), the phase transformation is first order, as manifested by the presence of thermal arrests (e.g., Fig. 3) in the cooling or heating curves, and by extremely sharp spikes in the heat-capacity curve at the transition temperature T_V. For the composition range $\delta_c<\delta<0.012$ (group-II specimens), the transition is of second or higher order, consistent with the absence of thermal arrests and with the broad heat-capacity anomalies near T_V. These distinctions are further substantiated by the following observations:

(a) Within experimental error, group-I and -II specimens share a common baseline above 126 K, as depicted by the representative plots in Fig. 5. This means that the nature of the spectrum of thermal fluctuations is the same well above T_V, irrespective of the character of the transition. The universality of the high-temperature behavior demonstrates that the lattice properties above T_V have not changed appreciably with increasing nonstoichiometry δ. However, below their respective T_V values this is no longer the case: the heat capacities for group-II specimens lie significantly above those for group-I specimens. This trend continues down to the lowest accessible temperature range of 5 and 0.3 K, as shown in Fig. 6 and in the work of Ref. 4, respectively. Below T_V changes in δ have a greater effect on the heat capacities of the second-order than on the heat capacities of the first-order samples. Clearly, the elementary excitations of the low-temperature phase of group-II samples increase with δ; they differ from those of group-I samples. This situation arises because, in type-II samples, as in any system undergoing a second-order transition, thermal fluctuations grow with T and destroy the ordered state at T_V. In type-I samples the transition is determined by the coexistence condition involving the equality of chemical potentials of the two stable phases.

(b) Within each grouping, T_V decreases linearly with increasing δ, as is shown in Fig. 7. T_V values shown as open circles were read off from either the average temperature of the thermal arrests for group-I specimens (as shown in Fig. 3) or from the maximum in the heat-capacity anomalies of group-II samples. T_V values shown as triangles were obtained from discontinuous temperature changes of the magnetic moment reported in detail elsewhere.[11] These transition temperatures interpolate satisfactorily with those read off from discontinuities in resistivities ρ or in $d\rho/dT$, obtained in complementary electrical transport measurements.[12] One clearly encounters two linear regions in the T_V versus δ dependence, with a gap in T_V extending from 109 to 101 K, which separates the transition temperatures of the first-order from those of the second-order regime. These findings provide a quantitative verification and extension of earlier observations,[13–16] including that by Verwey in his original report,[16] that T_V diminishes with increasing deviations of magnetite from the ideal oxygen stoichiometry.

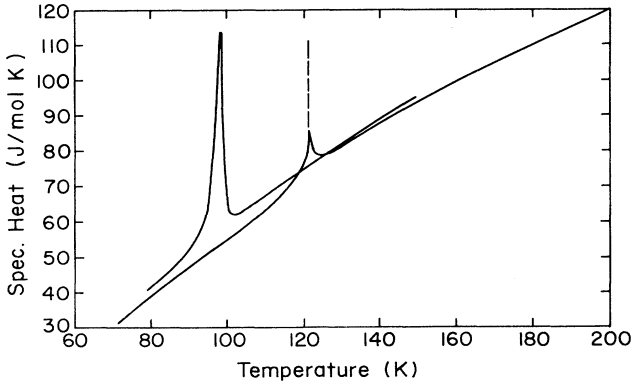

FIG. 5. Comparison of heat capacities for two samples exhibiting Verwey transitions of different order; $\delta=-0.000\,18$, first-order transition, and $\delta=0.0049$, second- or higher-order transition.

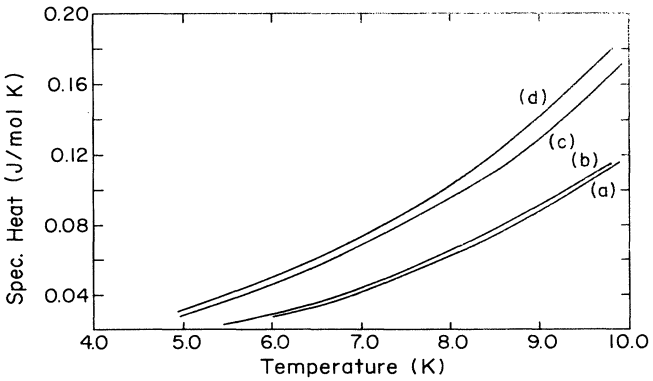

FIG. 6. Heat capacity vs temperature for several $Fe_{3(1-\delta)}O_4$ samples below 10 K. Curve (*a*): $\delta=-0.000\,18$; (*b*): $\delta=0.0002$; (*c*): $\delta=0.0096$; (*d*): $\delta=0.0121$.

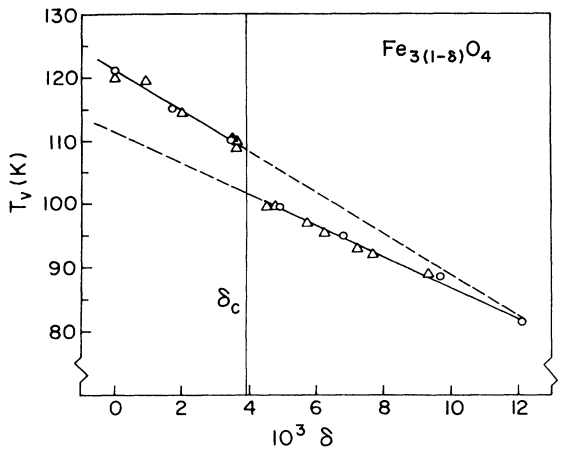

FIG. 7. Variation of Verwey transition temperature with δ in $Fe_{3(1-\delta)}O_4$. Note the two regimes and the separation of the temperature regions between 101 and 109 K. Circles refer to calorimetric measurements, triangles, to magnetic measurements.

(c) No offsets in baseline are encountered at the various first-order Verwey transitions: We find no experimental evidence to support claims[17] that short-range order always persists well above the Verwey transition temperature in this regime. In group-I samples the sharp heat-capacity spikes are superposed on top of small premonitory and postmonitory shoulders extending several degrees above and below T_V. The interpretation of these latter features is uncertain but their contribution to the transition enthalpy ΔH_V and entropy ΔS_V is estimated to be more than 1 order of magnitude below the corresponding values obtained from the thermal arrest curves.

(d) In the first-order regime the spikes in the heat-capacity anomalies were so sharp that they could not be fully tracked by the relaxation technique. Their positions, as read off from the thermal arrest curves, are indicated by dashed vertical lines in Fig. 1. In the second-order regime, the largest portion of the specific-heat anomaly extends over a 5–30 K temperature range below T_V; in principle, the anomaly occurs down to 0 K. The excess heat-capacity curve extends as well over a 5–15 K range beyond T_V, indicating that short-range ordering persists beyond the transition. The resultant curve forms a rather broadened λ-type trace, only roughly resembling that generally encountered in mean-field theories of second-order transitions. For the most cation-deficient specimen, $\delta=0.0121$, the ΔC_p versus T curve was nearly bell shaped. In this particular case a single-phase specimen could not be obtained by the quenching techniques described earlier. The areas under all ΔC_p curves in the temperature range above T_V represent a sizable fraction of the areas encountered in the range below T_V. Again, the precise shape of the excess ΔC_p curve such as in Fig. 4 depends greatly on how the base line is assumed to vary with temperature.

(e) No additional heat-capacity anomalies were detected below T_V for any of the samples. This finding is in agreement with earlier work in this laboratory[1–4] and elsewhere[15,18–20] on Fe_3O_4, but stands in contrast to an isolated report[21] of the onset of such an anomaly near 10 K.

(f) The entropies of transition ΔS_V calculated either from the thermal arrests of first-order samples by the methodology of Ref. 9, or from integration $\int(\Delta C_p/T)dT$ of the excess heat capacity ΔC_p in second-order specimens, are assembled in Tables I–III.

Table I summarizes various measured and calculated values pertaining to the Verwey transition in near-stoichiometric magnetite. The entropy of transition ΔS_V ranges from 5.63 to 6.08 J/(mol Fe_3O_4) K, with an average of 5.91 ± 0.06 J/(mol Fe_3O_4) K. This value does not include a contribution of ≈ 0.25 J/mol K associated with the premonitory and postmonitory effects that extend several K below and above T_V. As will be shown later, these findings are consistent with the modeling of the Verwey transition by a first-order change in electronic configuration, associated with an entropy difference

$$\Delta S_c = R\ \ln 2 = 5.763\ \text{J/mol}\ Fe_3O_4\ \text{K}\ .$$

TABLE I. Experimental results on the Verwey transition for stoichiometric Fe_3O_4. Values listed are the entropy of transition ($\pm$ variance), average transition temperature, upper limit on the width of the transition, hysteresis between heating and cooling transitions, and the total temperature difference that the sample traversed during the measurement.

Sample	ΔS (J/mol K)[a]	T_V (K)	Width (K)	Hysteresis (K)	ΔT (K)
1	5.88($\pm$0.05)	121.3	0.37	0.5	1.83
1	5.98($\pm$0.05)	120.8	0.49	0.5	2.22
2	5.98($\pm$0.14)	120.7	0.4	0.26	2.00
2	5.96($\pm$0.13)	120.5	0.5	0.26	2.00
2	5.84($\pm$0.07)	120.7	0.35	0.25	1.00
2	5.83($\pm$0.01)	120.5	0.35	0.25	1.00
3	6.08($\pm$0.03)	121.1	0.5	0.18	2.00
3	6.00($\pm$0.07)	120.9	0.5	0.18	2.00
3	5.63($\pm$0.09)	120.9	0.5	0.18	1.50

[a]Statistical error is shown. The experimental error is estimated to be below 5%. The contribution $\Delta S \approx 0.25$ J/mol K of Fe_3O_4 due to the premonitory and postmonitory effects is not included.

TABLE II. Experimental results on the discontinuous Verwey transition. Values listed are the deviation from stoichiometry δ, the entropy of transition ΔS_V (±variance), the average transition temperature, the upper limit on the width of the transition, hysteresis between heating and cooling transitions, and the total temperature difference the sample traversed during the measurement.

δ	S (J/mol K)[a]	T_V (K)	Width (K)	Hysteresis (K)	ΔT (K)
−0.0002	6.0(±0.1)	121.1(H)	0.3	0.2	2.00
−0.0002	6.0(±0.1)	120.9(C)	0.3	0.2	2.00
−0.0002	5.8(±0.1)	121.1(H)	0.3	0.2	1.83
−0.0002	5.6(±0.1)	120.9(C)	0.3	0.2	1.50
0.0002	5.9(±0.1)	120.7(H)	0.3	0.3	2.00
0.0002	5.8(±0.1)	120.4(C)	0.3	0.3	2.00
0.0002	5.8(±0.1)	120.7(H)	0.3	0.3	1.00
0.0002	5.8(±0.1)	120.4(C)	0.3	0.3	1.00
0.0007	5.6(±0.1)	119.4(C)	0.3	0.3	1.5
0.0007	5.6(±0.1)	119.7(H)	0.3	0.3	1.5
0.0017	5.3(±0.1)	115.8(H)	0.3	0.9	2.00
0.0017	5.3(±0.1)	114.9(C)	0.3	0.9	2.00
0.0017	5.2(±0.1)	115.8(H)	0.3	0.9	1.80
0.0017	5.1(±0.1)	115.8(H)	0.3	0.9	1.00
0.0017	5.1(±0.1)	114.9(C)	0.3	0.9	1.00
0.0035	4.0(±1)	110.7(H)	0.3	1.0	2.50
0.0035	4.0(±1)	109.7(C)	0.3	1.0	2.50

[a]Statistical error is shown. The experimental error is estimated to be below 5%. The contribution $\Delta \simeq 0.25$ J/mol K of Fe_3O_4 due to the premonitory and postmonitory effects is not included.

The difference between ΔS_c and ΔS_V is attributed to entropy alterations in the lattice, notably those due to the transition from the monoclinic to the cubic spinel phase. One should also take note of the very small hysteresis effects shown in Table I. The entropy differences quoted here lie well below those reported by previous investigators and are half of the quantity $2R$ ln2/mol Fe_3O_4 which had previously been thought to be correct. The present ΔS_c values appear to be more reliable because they were determined directly from thermal arrest data, whereas previously published entropies of transition were obtained from areas under artifically broadened heat-capacity plots. Actually, values close to $\Delta S_V = R$ ln2 had already been reported in Refs. 15 and 20, but the significance of these findings was not followed up. The variation of ΔS_V with δ and other data relating to the Verwey transition for nonstoichiometric specimens undergoing a first- or second-order transformation are collected in Table II or III. For reasons already mentioned, the entropy changes associated with the second-order Verwey transitions in Table III represent lower limits and are subject to considerable uncertainty. However, the general trend of a decreasing value in S_V in the neighborhood of T_V with increasing δ in the range $0.004 < \delta < 0.012$ is undoubtedly correct.

TABLE III. Experimental results on the continuous Verwey transition for $Fe_{3(1-\delta)}O_4$. Values listed are the deviation from stoichiometry, δ, the transition temperature, and the entropy of transition.

δ	T_V (K)	S (J/mol K)[a]
0.0049	97.5±0.5	1.73
0.0068	95.0±0.5	1.63
0.0096	89.0±0.5	1.78
0.0121	81.5±0.5	1.08

[a]Experimental errors are governed by the uncertainties of where the base line should be drawn and may thus be very large.

A variety of possible entropy changes at T_V are discussed in Appendix A, where we contrast models leading to the observed value $\Delta S_V = R$ ln2 with those appropriate to the larger limiting value of $2R$ ln2. Basically, the smaller ΔS_V may be derived on the assumption that, in Fe_3O_4, the Coulomb energy of repulsion between electrons on octahedral sites is much larger than the band energy appropriate to itinerant behavior of the carriers. On the other hand, when short-range order predominates, as in group-II specimens, the Coulomb interactions are largely screened out. One now predicts an entropy of transitions of $2R$ ln2 extending over the range $0 < T < T_V$. We attempted to verify this prediction by estimating the quantity $\int (\Delta C_p/T) dT$. Unfortunately, shifts in the base line by 5% (which is the experimental error) yielded fluctuations of the order of R ln2; hence, no conclusions could be drawn from an examination of the experimental data. The theoretical predictions are discussed further in Appendix B, where the finding that $\Delta S_V = R$ ln2 for first-order samples is also rationalized.

The variation of the entropy of $Fe_{3(1-\delta)}O_4$ over the entire temperature range from 0 to 300 K calculated from $S(T) = \int (C_p/T) dT$ as obtained by numerical integration is shown in Fig. 8 for one sample from group I ($\delta \simeq 0$) and for one from group II ($\delta \simeq 0.0121$), respectively. One should note that, below 120 K, $S_{\rm I}(T) < S_{\rm II}(T)$, where the subscripts here and later correspond to the two regimes.

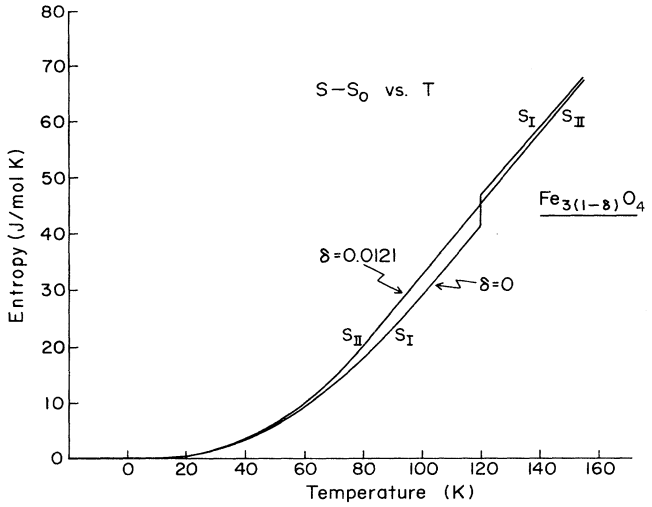

FIG. 8. Molar entropy of $Fe_{3(1-\delta)}O_4$ as a function of temperature for magnetite with $\delta=0$ and 0.0121.

The inequality shows that, at low temperatures, the lattice of the more nonstoichiometric magnetite is softer and subject to greater fluctuation effects. This observation is discussed further in Sec. IV. Above 120 K, $S_{II}(T)>S_I(T)$; this fact is explained in Appendix B where we show that the molar entropy change in samples of type I is R ln2, whereas it is $2R$ ln2 for those of type II.

IV. DISCUSSION

The above results are discussed under several headings.

(a) Experimentally, the first- and second-order regimes were encountered for δ values below 0.0035 and above 0.0049, respectively. The critical value δ_c marking the boundary between group-I and -II samples may be rationalized on the basis of the magnetite structure below T_V. In the monoclinic unit cell, let $n(I)$ and $n(V)$ be the number of interstitial cations and cation vacancies, respectively, and let

$$n(\Sigma)=n(\mathrm{Fe}^{2+})+n(\mathrm{Fe}^{3+})+n(V) .$$

Then

$$\delta=[n(V)-n(I)]/n(\Sigma) .$$

The electroneutrality condition for nonstoichiometric magnetite requires[22] that

$$n(V)-n(I)=[n(\mathrm{Fe}^{3+})-2n(\mathrm{Fe}^{2+})]/8 ,$$

whence,

$$\delta=[n(\mathrm{Fe}^{3+})-2n(\mathrm{Fe}^{2+})]/8n(\Sigma) .$$

Oxidation of one Fe^{2+} to an Fe^{3+} ion changes the difference

$$[n(\mathrm{Fe}^{3+})-2n(\mathrm{Fe}^{2+})]$$

by 3. The monoclinic unit cell of magnetite contains 32 formula units of Fe_3O_4, so that $n(\Sigma)=96$. Substitution of these values into the expression for δ yields $\delta_c=0.0039$, which falls comfortably in the range of experimental observation. Thus, conditions for a first-order phase change apparently can no longer be maintained when, on the average, one of the 32 ferrous ions per unit monoclinic cell is converted to the ferric state through the incorporation of excess oxygen into the lattice.

(b) A consistent framework for interpretating the experimental observations in both the first- and second-order regimes may be provided by the phenomenological model of Strässler and Kittel[23] (SK) who generalized the treatment of regular solution theory. The adaptation of their approach to the Verwey transition was discussed in detail by Aragón and Honig,[24,25] and was further elucidated in a recent publication by Honig and Spałek[26] in which the SK model was derived as a limiting case of a microscopic model including intracell Coulomb interaction between electrons. The basic concepts need only be briefly summarized; the principal ingredients of the microscopic approach[26] are briefly sketched out in Appendix B. In the SK approach, one simulates the interaction among electrons in magnetite by a quasi-two-level system involving ground and excited states of energy 0 and ε, with degeneracy g_0 and g_1, respectively. The state of the system at temperature T is characterized by an order parameter ψ, representing the fraction of constituents in the excited state. One expands the internal energy E to quadratic terms in ψ; i.e., $E=N(\varepsilon\psi-\lambda\psi^2/2)$, where N is the total number of subunits and λ is an interaction energy parameter. This is a standard expression for the electron energy, containing both the single-particle ($\varepsilon\psi$) and interaction ($-\frac{1}{2}\lambda\psi^2$) energies, for a uniform system with charge carrier density ψ. The quantity E is then combined with the usual expression for the entropy of $N(1-\psi)$ and $N\psi$ subunits among the ground and excited states with their respective degeneracies. One thereby arrives at an expression of the free energy

$$\begin{aligned} F/N&=(E-TS)/N \\ &=\varepsilon\psi-(\lambda/2)\psi^2 \\ &\quad -k_BT[\psi\ln g_1+(1-\psi)\ln g_0 \\ &\qquad -\psi\ln\psi-(1-\psi)\ln(1-\psi)] . \end{aligned} \tag{1}$$

Equilibrium is characterized by the constraint $\partial(F/N)/\partial\psi=0$ which leads to the condition

$$\varepsilon-\lambda\psi=k_BT\{\ln(g_1/g_0)+\ln[(1-\psi)/\psi]\} \tag{2}$$

that must be met by a model system characterized on the basis of the above mean-field theory. A general analysis[24] shows that $\varepsilon-\lambda\psi<0$, thus forcing a transition. Equation (2) may be solved numerically for the long-range order parameter

$$\psi=\psi(T;\varepsilon,\lambda,g_1/g_0) .$$

Transitions are either first order, second order, or nonexistent according as $g_1/g_0>1$, $g_1/g_0\geq 1$, or $g_1/g_0<1$; thus, the various possibilities are encompassed within a single phenomenological scheme. From the description of the microscopic model the *ad hoc* parameters g_0 and g_1 are determined explicitly rather than remaining as ad-

justable parameters.

The parametrization procedure for the determination of ε, λ, and g_1/g_0 in terms of the stoichiometry parameter δ has been described in detail in Ref. 24; the scheme invokes the T_V versus δ dependence of Fig. 7. Within the microscopic model,[26] the values $g_1/g_0=2$ or 1 required for first- or second-order transitions are obtained automatically; the theory also reproduces the experimental fact that the entropy of the Verwey transition of stoichiometric magnetite is given by $\Delta S_V=R\ln 2$; see also, Appendix B.

Having obtained $\psi(T;\varepsilon,\lambda,g_1/g_0)$ for each sample, one can determine the entropy for each first-order transition from the relation

$$\begin{aligned}\Delta S_V/kN&=[S(\psi_+)-S(\psi_-)]/kN\\&=(\psi_+-\psi_-)\ln(g_1/g_0)-(\psi_+\ln\psi_+-\psi_-\ln\psi_-)\\&\quad+[(1-\psi_+)\ln(1-\psi_+)\\&\quad-(1-\psi_-)\ln(1-\psi_-)]\,,\end{aligned}\tag{3}$$

where ψ_+ or ψ_- are the values of ψ calculated via Eq. (2) for temperatures just above or below the first-order phase transition at T_V. The solid curve in Fig. 9 shows the values of $\Delta S_V/R\ln 2$ versus δ determined from (3), while the circles represent the corresponding experimental data. One should note that $\Delta S_V\neq 0$ for $\delta=\delta_c$, which corresponds to the fact that, under the existing experimental conditions, the discontinuity $\psi_+-\psi_-$ remains nonzero as the critical value δ_c is approached from below. The experimental trend is thus satisfactorily reproduced by the mean-field theory.

(c) From $\psi(T;\varepsilon,\lambda,g_1/g_0)$ one may also determine, via Eq. (1), the variation of heat capacity $C=(\partial E/\partial T)$ and entropy S due to changes in the order parameter with temperature both below and above T_V. As anticipated, these curves resemble the corresponding functions which arise in the standard mean-field theory of discontinuous and continuous transitions.

It is difficult to attempt a direct comparison between the calculated and experimental heat-capacity curves because the SK approach deals solely with the electron repopulation among shifting energy levels as a function of T, whose effect is especially marked near T_V. By contrast, the experimental results additionally include contributions involving the lattice, and the magnetic degrees of freedom. All of the above properties change significantly near the Verwey transition temperature. What is noteworthy is that, below $\sim$55 K for group-I specimens and $\sim$40 K for group-II specimens, the contribution to C_p due to configurational changes as determined by the SK theory is very small.

We next discuss the entropies which are much less sensitive than C_p to temperature variations. Figure 10 shows the calculated configurational (SK) entropies $S_{\rm I}^c$ or $S_{\rm II}^c$ based on Eq. (1) as applied to $Fe_{3(1-\delta)}O_4$ with $\delta=0$ or 0.012, respectively.

The calculated $S_{\rm I}^c(T)$ or $S_{\rm II}^c(T)$ values displayed in Fig. 10 approach 60% of the $S_{\rm I}(T)$ or $S_{\rm II}(T)$ curves shown in Fig. 8, close to the respective Verwey transitions. To gain a further perspective on the calculated configurational entropy $S_{\rm II}^c(T)$ relative to the experimental entropy $S=\int(C_p/T)dT$, we show, in Fig. 11, a calculation of S that can be directly compared with experiment. This involves the determination of $S_{\rm II}^c(T)$ by use of the multiplier of T in Eq. (1) with $g_1=g_0=1$ and the Debye lattice contribution to the entropy $S_{\rm II}^L(T)$ in terms of the Debye constant $\Theta_D=511$ K specified in Ref. 4. The dashed curve in Fig. 11 represents $S_{\rm II}^c$; the dot-dashed curve is calculated as $S_{\rm II}^L=\psi\int(C_p/T)dT$. The factor ψ was introduced because $1-\psi$ represents that portion of the electron (and lattice) subsystem which is in a frozen configuration. Hence, only the fraction ψ of the system contributes to thermal changes in the system. The $S_{\rm II}^c$ contribution to $S_{\rm II}$ reaches a maximum of 60% at $T_V=85$ K. One may then ask why the pronounced kink seen in the S_c curve of Fig. 11 at 85 K does not result in an attenuated anomaly centered on 85 K in the experimental $S_{\rm II}$ curve shown in Fig. 8. Two principal

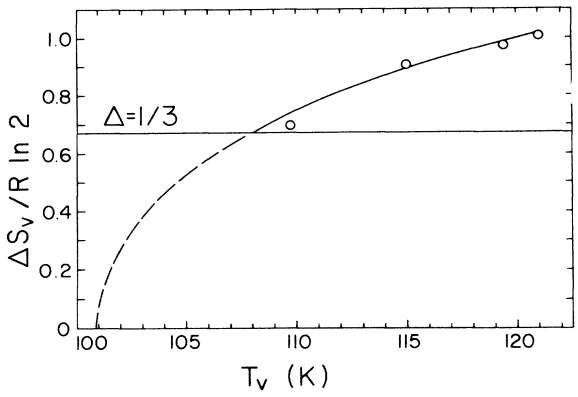

FIG. 9. Entropy of first-order Verwey transition ΔS_V vs T_V for magnetite samples with $0\leq\delta<0.004$. Circles represent experimental data, curve shows results of theoretical calculation based on Eq. (3).

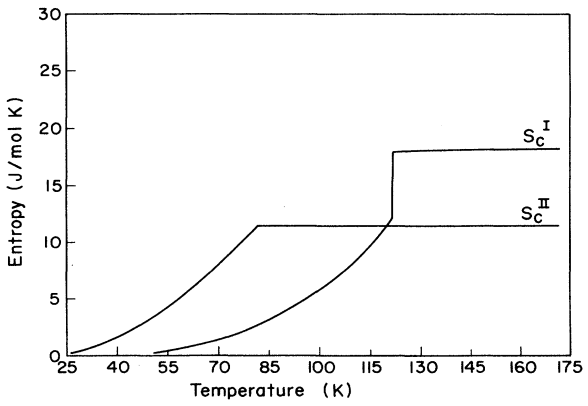

FIG. 10. Calculated variation of S vs T due to electronic configurational effects by use of the SK mean-field theory. $S_{\rm I}^c$ and $S_{\rm II}^c$ refer to group-I and group-II samples.

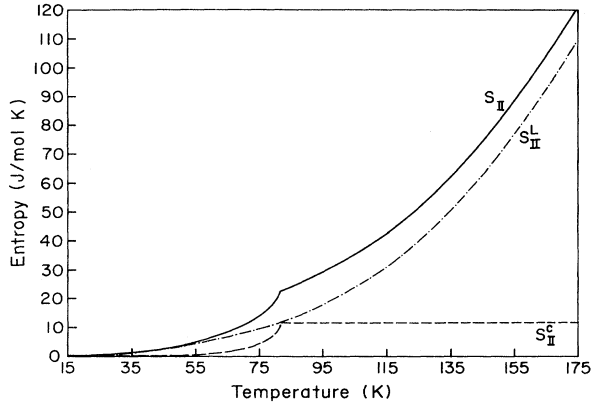

FIG. 11. Calculation of entropy as a function of temperature. Dotted curve represents $S_{II}^{c}(T)$ as determined by Eq. (1). Dashed curve represents $S_{II}^{L}(T)$ calculated as described in the text. Solid curve is the total calculated entropy.

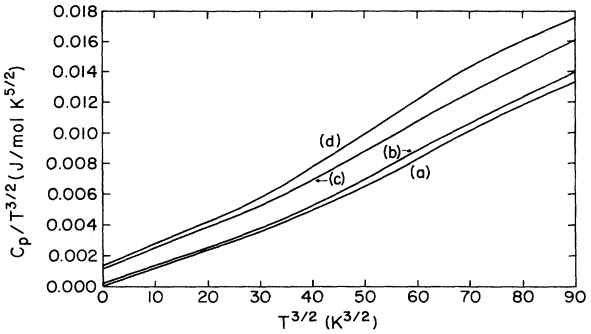

FIG. 12. Plot of $C_p/T^{3/2}$ vs $T^{3/2}$ for $Fe_{3(1-\delta)}O_4$ for samples with different δ. Curve (a), $\delta=-0.000\,18$; curve (b), $\delta=0.0049$; curve (c), $\delta=0.0096$; curve (d), $\delta=0.0121$.

reasons may be cited. First, as pointed out in Ref. 26, the lattice itself relaxes significantly; the local deformations around the localized electrons of the low-temperature monoclinic phase are eliminated as T_V is approached from below. Numerical estimates based on a softening of one of the lattice optic modes near T_V have shown that there is a sudden small increase in the lattice entropy which tends to round off and stretch the kink in S_{II}^{c}. Second, and more important, one must recognize that the mean-field SK calculations of S_{II}^{c} are highly approximate near T_V because they fail to deal with fluctuations that become prominent near the critical temperature of any second-order phase transition. As Figs. 2 and 4 clearly show, the experimental heat-capacity anomalies do not terminate sharply at T_V, as would be the case for the ordinary λ-type transition. Thus, fluctuations and/or short-range-order effects induced by spatial disorder when $\delta>\delta_c$ smear out the mean-field discontinuities in C_p to such an extent that S_{II} continues to vary smoothly with T even near T_V. These order-parameter fluctuations are intrinsically absent in systems undergoing first-order transitions; thus, the predictions of mean-field theory for $\delta<\delta_c$ are expected to provide a very good approximation to the actual configurational entropy contributions. This is the reason why the first-order theory and experiment are in excellent accord, as is verified by Fig. 9 and by other comparisons between theory and experiment.[24,25,27]

(d) The spin-wave excitations in Fe_3O_4 at very low temperatures have also been investigated as a follow-up effort on our recent study[4] in the range 0.3–10 K; in the present work the measurements were extended to 30 K. Since these later studies are similar to the earlier ones, they will be described only briefly. The asymptotic low-temperature form for the heat capacity is given by $C_p=AT^{3/2}+BT^3$, where the two terms deal, respectively, with magnon and phonon excitations. Plots of $C_p/T^{3/2}$ versus $T^{3/2}$ for the latter data were found to yield two linear portions, with a break at 10 K, as shown in Fig. 12. Similar findings were reported by Gmelin *et al.*[15] The significance of this effect is not understood but it appears to be related to an anomaly also detected in this temperature range in studies of the magnetoelectric effect.[28] The slopes and intercepts of the curves in Fig. 12 in the 5–10 K range agree reasonably well with those reported earlier,[4] whereas values read off from the data in the 10–30 K range of Fig. 12 are significantly higher. This is consistent with the general observation that the Debye parameter Θ_D is found to vary significantly with temperature above 10 K. Hence, earlier literature values for the Debye temperature and magnetic exchange constants of Fe_3O_4, which were based on data in the higher-temperature range, may be in need of revision.

V. SUMMARY AND CONCLUSIONS

On the basis of systematic heat-capacity studies involving $Fe_{3(1-\delta)}O_4$ with $-0.0005<\delta<0.012$, we have provided further proof that the Verwey transition changes from first to second or higher order as δ is increased past the critical value $\delta_c=0.0039$. Correspondingly, the entropy of transition is given by $\Delta S_V=R\ln 2$ for $\delta=0$ and diminishes with rising δ (cf. Fig. 9). Also, the Verwey transition temperature T_V drops linearly with rising δ; there is a discontinuity both in T_V and in its slope at $\delta=\delta_c$ (cf. Fig. 7). Differences in heat capacity for the first- and second-order samples persist down to the cryogenic temperature range. Finally, the magnon contribution to the specific heat in the range below 10 K is found to differ from that above 10 K.

The above observations are rationalized in terms of an elementary model (Appendices A and B) in which the Coulomb interaction between electrons placed on neighboring octahedral sites is gradually screened out with increasing departures from ideal stoichiometry. The microscopic model is sketched out in the Appendices; it leads directly to the Strässler-Kittel formalism [Eqs. (1)–(3)]. The latter has been used by us to describe and interpret both the first- and the second-order transitions within one consistent framework: in the neighborhood of the Verwey transition, the electron population is shifted either discontinuously or continuously among two levels.

A more comprehensive theoretical analysis which also includes transport phenomena is to be presented elsewhere.

ACKNOWLEDGMENT

This research was supported by National Science Foundation Grant No. DMR-86 16533.

APPENDIX A: ACCESSIBLE CONFIGURATIONS AND ENTROPY OF ELECTRONS LOCATED ON OCTAHEDRAL SITES

We simulate magnetite in a simple manner via a collection of $2N$ octahedral sites per mole of Fe_3O_4, where N is Avogadro's number. (The formal decomposition into pair-site subunits is discussed in Appendix B.) These sites may be populated by cations in either the Fe^{3+} (d^5) or the Fe^{2+} (d^6) configuration. To take account of variations in energy which depend on the valence states of nearest-neighbor cations, we consider pairs of adjacent octahedral sites for stoichiometric Fe_3O_4 for which, on the average, one ion is in the Fe^{2+} and the other ion, in the Fe^{3+} configuration. We encounter 16 pair states shown in the top section of Table IV. Here the spin ($\sigma=\pm1$) configurations of the extra electron forming Fe^{2+} from a Fe^{3+} "core" state are indicated by corresponding arrows, while the Fe^{3+} spin-aligned $3d^5$ state is regarded as a vacuum (0) state. We consider the high-spin configuration $S=\frac{5}{2}$ of the Fe^{3+} $3d^5$ "core" state as frozen since $T_V \ll T_C \approx 950$ K, where T_C is the Curie temperature.

The entropy connected with such a set of noninteracting electron states for an ensemble of pairs is

$$S=2k_BN\sum_{\sigma}[n_\sigma \ln n_\sigma+(1-n_\sigma)\ln(1-n_\sigma)] , \qquad \text{(A1)}$$

where n_σ is the probability of encountering a typical site with an extra electron (i.e., an Fe^{2+} ion) in the spin state σ. For stoichiometric magnetite $n_\sigma=\frac{1}{2}$, whence $S=4R\ln2$, corresponding to the random occupancy of octahedral sites with equal probabilities, as shown in Table II.

In actuality, such random occupancy is not possible because the sixth d electron on Fe^{3+} must have its spin aligned antiparallel to the $S=\frac{5}{2}$ spin state of the five remaining electrons. Moreover, below the Curie point, these d^5 spins are themselves aligned, thereby defining a macroscopic magnetization $M\approx5\mu_B/Fe^{3+}$ ion. This type of ferromagnetic ordering restricts the occupancies to the much more limited set of four states shown in the middle section of Table IV, and corresponds to setting $n_\uparrow=\frac{1}{2}$ and $n_\downarrow=0$. The summation over $\sigma=\pm1$ in Eq. (A1) must now be dropped; one then obtains the result

$$S=2R\ln2/\text{mol}\,Fe_3O_4 .$$

This is the value anticipated for the second-order transition; however, it is still too large by a factor of 2 to account for the change $\Delta S_V=R\ln2$ at the first-order Verwey transition.

So far the interactions between the extra electrons on adjacent Fe^{2+} ions have been ignored. In our view this is not plausible in a system characterized by long-range order: Fe_3O_4 is a semiconductor at high temperature, which indicates that the extra d electrons on Fe^{2+} that are involved in the electric conduction remain almost localized (had a band been formed, it would have been quarter filled). To keep the electrons from forming a band, the Coulomb repulsion energy must always be much larger than the single-particle energy. In such a situation, the third of the configuration shown in the middle section of Table IV is no longer accessible; correspondingly, the third and fourth configurations must now be dropped. The remaining available configurations in the limits of very strong Coulomb repulsions are shown in the bottom section of Table IV. The conventional Fermi-Dirac (FD) statistical distribution function is also no longer applicable to this case. The appropriate distribution which takes its place has been discussed in detail by Spałek and Wójcik[29] and leads directly to the same expression as that for distribution of electrons in single-electron donor states in semiconductors. With this altered distribution function for the accessible configurations specified in the bottom section of Table IV, one obtains an entropy expression which replaces Eq. (A1), from which one finds that $S=R\ln2/\text{mol}\,Fe_3O_4$, in conformity with the result obtained intuitively on comparing the number of available configurations in the bottom section of Table IV with those of the middle section of Table IV.

One should also note that, for nonstoichiometric magnetite, $3\delta.2N$ additional Fe^{3+} ions have been generated per mole of Fe_3O_4. Hence, the corresponding entropy change for nonstoichiometric magnetite should be smaller, as is, in fact, demonstrated by Fig. 9.

Thus, the expression for the change entropy connected with the Verwey transition $\Delta S_V=R\ln2$ for stoichiometric Fe_3O_4, is obtained on the assumption that,

TABLE IV. Possible occupation states of a single orbital octahedral pair of sites.

Random states configurations:			All states
↑	0	0	0
0	↑	↑↓	0
↓	0	0↓	↑
0	↓	↑↓	↑
↑	↑	↑↓	↓
↓	↓	↑	↓↑
↑	↓	↓	↑↓
↓	↑	↑↓	↑↓
Configurations in spin-ordered situation			
↑	0		
0	↑		
↑	↑		
0	0		
Accessible states for strong intracell interactions			
↑	0		
0	↑		

well below T_V, all electrons are in a single frozen configuration, and that above T_V they are in configurations that avoid Fe^{2+}-Fe^{2+} and Fe^{3+}-Fe^{3+} pair formation on adjacent octahedral sites. The present discussion is, of course, very much oversimplified since we calculate the entropy in the atomic limit. A more realistic treatment is provided in a recent article.[26] Additional information is supplied in Appendix B.

APPENDIX B: SUMMARY OF MICROSCOPIC ANALYSIS LEADING TO THE STRÄSSLER-KITTEL MODEL

We briefly describe the theory developed by Honig and Spałek[26] from which the SK model may be derived. Consider Fe^{2+} and Fe^{3+} ions on $2L$ octahedral sites in Fe_3O_4. The Fe^{3+} core is regarded as the vacuum state, and the L electrons forming Fe^{2+} out of the Fe^{3+} state are assumed to determine the entire dynamics of the transition. Consequently, we ignore the "core" Fe^3 states and concentrate only on the L electrons distributed among octahedral sites. To take account of interaction octahedral sites, we group them into $N=ZL/2$ pairs (bonds). In the ground state with zero energy ($T\to 0$), one electron per bond is frozen in an ordered state, consistent with a lattice deformation, whose periodicity produces the monoclinic distortion. There then exists a state of intermediate energy ε where the electron resonates between the two equivalent sites of the bond; this is the precursor to the conduction process that occurs in the presence of an applied electric field. There further exists a state of higher energy U corresponding to the case where two electrons reside on two neighboring octahedral sites.

The four possible configurations are schematized in Table V. Since Fe_3O_4 is a semiconductor both above and below T_V, we infer that U greatly exceeds the electron-transfer integral. We now show that the change of nature of the Verwey transition versus δ requires a strong reduction of U with growing δ.

The free energy of the bond assembly shown in Table V is given by[26]

$$F/N=[2\varepsilon\alpha_1+(U-2\varepsilon)\beta_2] -k_BT[(1-2\alpha_1+\beta_2)\ln(1-2\alpha_1+\beta_2) +2(\alpha_1-\beta_2)\ln(\alpha_1-\beta_2)+\beta_2\ln\beta_2]\ , \quad \text{(B1)}$$

where $\alpha_1\equiv\beta_1+\beta_2$ is the probability that a given site contains an electron in the resonant state, and where the β_j are the occupation probabilities shown in Table V. The first two terms in square brackets represent the energy; the multiplier of T represents the electronic part of the entropy.

Minimizing F/N with respect to β_2 yields

$$(1-2\alpha_1+\beta_2)\beta_2/(\alpha_1-\beta_2)^2=\exp(-R/k_BT) \quad \text{(B2)}$$

with $R\equiv-(U-2\varepsilon)+2\varepsilon'\alpha_1-(U'-2\varepsilon')\beta_2$; primes denote differentiation with respect to β_2. The optimized free energy then becomes

$$F/N=2\varepsilon\alpha_1+2\varepsilon'\beta_2(\alpha_1+\beta_2)-U'\beta_2^2 +k_BT[(1-2\alpha_1)\ln(1-2\alpha_1+\beta_2) +2\alpha_1\ln(\alpha_1-\beta_2)]\ . \quad \text{(B3)}$$

To solve this equation one must specify the dependence of ε and U as a function of β_2. In what follows we consider only the two limiting situations $U\to\infty$ and $U\to 0$. The general discussion of (B3) is deferred to a separate publication.

1. Case *A*: $U\to\infty$ ($R\to\infty$)

In this situation $\beta_2=0$, $\alpha_1=\beta_1$; we also introduce an order parameter $\psi\equiv 2\beta_1$. Then Eq. (B3) reduces to the special case

$$F/N=\varepsilon(\psi)\psi+k_BT[(1-\psi)\ln(1-\psi)+\psi\ln\psi-\psi\ln 2]\ , \quad \text{(B4)}$$

which is the starting relation for ψ within the Strässler-Kittel formalism that was used[24] to describe the discontinuous Verwey transition in the linear approximation $\varepsilon(\psi)=\varepsilon_0-\frac{1}{2}\lambda\psi$. Equation (B4) is equivalent to Eq. (1) with $g_1=2$, $g_0=1$. The minimization of Eq. (B4) with respect to ψ produces a jump in the ψ value from $\frac{1}{4}$ to $\frac{3}{4}$ at the transition. The corresponding entropy change is $R\ln 2$ per mole of Fe_3O_4.

2. Case *B*: $U\to 0$ ($R\to 0$)

Here $\beta_2=\alpha_1^2$; the appropriate order parameter is $\psi\equiv\alpha_1$ and the free energy per site is obtained from Eq. (B3) as

$$F/2N=\varepsilon(\psi)\psi+k_BT[(1-\psi)\ln(1-\psi)+\psi\ln\psi]\ , \quad \text{(B5)}$$

which has been used[24] as a starting point within the Strässler-Kittel formalism to describe the second-order

TABLE V. Possible configurations of the Fe ion pair of octahedral sites in stoichiometric magnetite.

Designation	Representation		Energy	Probability	Ionic state
AA	○	○	$\varepsilon_{AA}\equiv 0$	β_0	$Fe^{3+}+Fe^{3+}$ +trapped electron
AB	○	●	$\varepsilon_{AB}\equiv\varepsilon$	$2\beta_1$	Fe^{3+}-Fe^{2+}
BA	●	○	$\varepsilon_{BA}\equiv\varepsilon$		Fe^{2+}-Fe^{3+}
BB	●	●	$\varepsilon_{BB}\equiv U$	β_2	Fe^{2+}-Fe^{2+}

Verwey transition in the linear approximation $\varepsilon(\psi)=\varepsilon_0-\frac{1}{2}\lambda\psi$. Equation (B5) is equivalent to Eq. (1) with $g_0=g_1=1$. Thus, a rather simple, purely electronic, model properly describes the two regimes of interest. The minimization of F with respect to ψ leads to the solution $\psi=\frac{1}{2}$ for T above the continuous transition. Therefore, the entropy change per pair of octahedral sites associated with the transition is equal to 2 ln2, or equivalently, $2R$ ln2 per mole of Fe_3O_4. Details are provided in Ref. 26 and are also to be published separately.

---

*Present address: Kodak Research Laboratories, Rochester, NY 14650-2011.

†Present address: Department of Chemical Engineering, Colburn Laboratory, University of Delaware, Newark, Delaware 19716.

‡On leave from Department of Solid State Physics, AGH Technical University, 30-059 Kraków, Poland.

[1]J. P. Shepherd, J. W. Koenitzer, R. Aragón, C. J. Sandberg, and J. M. Honig, Phys. Rev. B **31**, 1107 (1985).

[2]J. P. Shepherd, J. W. Koenitzer, C. J. Sandberg, R. Aragón, and J. M. Honig, J. Mol. Cryst. Liq. Cryst. **107**, 191 (1984).

[3]J. P. Shepherd, R. Aragón, J. W. Koenitzer, and J. M. Honig, Phys. Rev. B **32**, 1818 (1985).

[4]J. W. Koenitzer, P. H. Keesom, and J. M. Honig, Phys. Rev. B **39**, 6231 (1989).

[5]H. R. Harrison and R. Aragón, Mater. Res. Bull. **13**, 1097 (1978).

[6]R. Dieckmann, Ber. Bunsenges. Phys. Chem. **86**, 112 (1982).

[7]R. Dieckmann and H. Schmalzried, Ber. Bunsenges. Phys. Chem. **81**, 344 (1977); **81**, 414 (1977).

[8]J. Crank, *The Mathematics of Diffusion* (Clarendon, Oxford, 1975).

[9]B. F. Griffing and S. A. Shivashankar, Rev. Sci. Instrum. **49**, 549 (1980).

[10]B. F. Griffing and S. A. Shivashankar, Rev. Sci. Instrum. **48**, 1255 (1977).

[11]Z. Kąkol and J. M. Honig, Solid State Commun. **70**, 967 (1989).

[12]R. Aragón, R. J. Rasmussen, J. P. Shepherd, J. W. Koenitzer, and J. M. Honig, J. Magn. Magn. Mater. **54-57**, 1335 (1986).

[13]R. Aragón, D. J. Buttrey, J. P. Shepherd, and J. M. Honig, Phys. Rev. B **31**, 430 (1985).

[14]R. Aragón, J. P. Shepherd, J. W. Koenitzer, D. J. Buttrey, R. J. Rasmussen, and J. M. Honig, J. Appl. Phys. **57**, 3221 (1985).

[15]E. Gmelin, N. Lenge, and H. Kronmüller, Phys. Status Solidi A **79**, 465 (1983).

[16]E. J. W. Verwey, Nature **144**, 327 (1939).

[17]D. Ihle and B. Lorenz, Phys. Status Solidi B **63**, 599 (1974).

[18]E. F. Westrum, Jr. and F. Grønvold, J. Chem. Thermodyn. **1**, 543 (1969).

[19]M. O. Rigo, J. F. Mareche, and V. A. M. Brabers, Philos. Mag. B **48**, 421 (1983).

[20]G. B. Falk, L.-S. Pan, B. J. Evans, and E. F. Westrum, Jr., J. Chem. Thermodyn. **11**, 367 (1979).

[21]S. Todo and S. Chikazumi, J. Phys. Soc. Jpn. **43**, 1091 (1977).

[22]R. Aragón and R. H. McCallister, Phys. Chem. Miner. **8**, 112 (1982).

[23]S. Strässler and C. Kittel, Phys. Rev. **139**, A758 (1965).

[24]R. Aragón and J. M. Honig, Phys. Rev. B **37**, 209 (1988).

[25]J. M. Honig, Phys. Chem. Miner. **15**, 476 (1988).

[26]J. M. Honig and J. Spałek, J. Less Common Met. **156**, 423 (1989); J. M. Honig, J. Spałek, and P. Gopalan (unpublished).

[27]J. M. Honig and P. Gopalan, Solid State Ionics **32-33**, 802 (1989).

[28]Y. Miyamoto, M. Ariya, A. Otuka, E. Morita, and S. Chikazumi, J. Phys. Soc. Jpn. **46**, 1947 (1979).

[29]J. Spałek and W. Wójcik, Phys. Rev. B **37**, 1532 (1988).